Journal of ELECTRONIC MATERIALS
DOI: 10.1007/s11664-015-4078-9

Two-Step Reactive Aid Sintering of $BaZr_{0.8}Y_{0.2}O_{3-\delta}$ Proton-Conducting Ceramics

SIWEI WANG,[1] YAN CHEN,[2] LINGLING ZHANG,[3] CONG REN,[1] FANGLIN CHEN,[3,4] and KYLE S. BRINKMAN[1,5]

1.—Department of Materials Science and Engineering, Clemson University, Clemson, SC 29634, USA. 2.—Chemical and Engineering Materials Division, Oak Ridge National Laboratory, Oak Ridge, TN 37831, USA. 3.—Department of Mechanical Engineering, University of South Carolina, Columbia, SC 29208, USA. 4.—e-mail: chenfa@cec.sc.edu, 5.—e-mail: ksbrink@clemson.edu

Ceramic-based proton conductors enable high-temperature hydrogen economy applications such as hydrogen separation membranes, fuel cells, and steam electrolyzers. $BaZr_{0.8}Y_{0.2}O_{3-\delta}$ (BZY) proton-conducting oxide possesses the highest level of proton conductivity reported to date, but poor sinterability hinders its widespread utilization. In this paper, we report a two-step reactive aid sintering (TRAS) method involving the introduction of $BaCO_3$ and B_2O_3-Li_2O for the preparation of dense BZY ceramics sintered at 1500°C. The resulting BZY samples showed a pure perovskite structure with a dramatic increase in the relative density to 91.5%. In addition, the shrinkage during sintering was improved to 19.3% by a TRAS method as compared to 2.6% by the conventional solid date reaction method. The bulk conductivity was improved due to enhanced densification, while the grain boundary conductivity decreased due to the blocking behavior of the sintering aid resulting in a decrease in the total conductivity of the samples.

Key words: Proton conductor, solid oxide fuel cells, sinterability, solid-state reactive sintering, sintering aid

INTRODUCTION

Proton-conducting oxides are a promising class of ceramic materials for energy conversion and storage applications, such as proton-conducting solid oxide fuel cells, high-temperature hydrogen separation membranes, and steam electrolyzers.[1–9] There are two main types of perovskite oxides that are currently used for these applications: doped cerates and doped zirconates. The doped cerates such as rare earth-doped $BaCeO_3$ and $SrCeO_3$ have demonstrated very high conductivity in humidified atmospheres as well as good sinterability. However, these materials possess poor thermodynamic stability towards water and CO_2; consequently their potential application is strictly limited.[10] On the contrary, doped $BaZrO_3$ is thermodynamically more stable than the cerate counterpart, which has attracted increased attention in recent years. However, the refractory nature of zirconium makes the $BaZrO_3$ -based materials very difficult to densify. A nominal sintering temperature of above 1700°C requires the use of a special high-temperature furnace and may lead to unfavorable evaporation of Ba from the A-site.[11,12]

To overcome these drawbacks, several methods aimed at improving sinterability, while maintaining the conductivity of doped $BaZrO_3$ have been attempted including the addition of sintering aids, as well as utilization of new sintering methods. Haile's group has reported ZnO-added BZY prepared by a wet chemistry method.[13] The sintering temperature was reduced to 1300°C with a surface grain size in the range of 1 μm. Irvine's group has also developed ZnO-doped BZY by a solid state reaction (SSR) method with a calcination temper-

(Received June 25, 2015; accepted September 18, 2015)

Published online: 14 October 2015

ature of 1400°C and a final sintering temperature of 1325°C.[14,15] CuO-doped BZY was also densified at 1600°C with an average grain size of 0.5–1 μm.[16] Bi_2O_3 was also reported to improve the densification of BZY.[17] Here, in this report, we introduced B_2O_3-Li_2O as a liquid-phase sintering aid for BZY-based ceramics. This type of sintering aid has been used in the dielectric and ferroelectric area, but not in the field of proton-conducting ceramics.[18,19] The sintering temperature of $BaZr_{0.35}Ti_{0.65}O_3$ was lowered from 1500°C to 1000°C by introducing a 4.75 wt.% B_2O_3-Li_2O sintering aid.[18] However, the sintering aid should be carefully chosen with regards to the overall defect chemistry of the BZY system.[20]

Processing modifications, such as the use of a reactive sintering method, have been adopted to improve the densification as well as grain growth in BZY materials. The reactive sintering method is a recently developed sintering method, where the reaction occurs during the sintering process, with some of the reactants (or transition/secondary phases) functioning as sintering aids. Tong et al. introduced NiO directly into the oxide precursors of BZY to sinter dense ceramics, with the transition phase BaY_2NiO_5 functioning as the sintering aid. Grain sizes as large as 5 μm were achieved after sintering at 1500°C for 24 h.[8,21] Chen et al. further found that BaY_2NiO_5 was formed as a secondary phase after sintering, and transformed to Ni metallic particles after being treated in a wet reducing atmosphere at high temperature.[7] This reactive sintering method has been verified by Ricote by obtaining BZY pellets with 1.3-μm grain size after sintering at 1500°C for 4 h.[22] Haile's group developed a similar reactive sintering method without using a sintering aid, but rather utilizing $BaCO_3$ as a precursor.[23] The existence of $BaCO_3$ at a calcination temperature of 850°C by the sol–gel method improved the sinterability of BZY, resulting in a grain size of 1.4 μm after sintering at 1600°C for 24 h.[23] The conductivity was significantly improved since no extra sintering aid was introduced; however, this sintering temperature is still too high for most applications.

In this study, we introduce a two-step reactive aid sintering (TRAS) method to BZY ceramic sintering that combines the advantage of sintering aid methods and reactive sintering. The sample was initially sintered by a reactive sintering strategy at an intermediate temperature, showing a relatively large grain size with a residual porous microstructure. Subsequently, the sample was ground into powder and the B_2O_3-Li_2O (B-Li) sintering aid was added to enhance grain boundary diffusion via formation of a liquid phase at the grain boundary. The samples were finally sintered at 1500°C, targeting dense, large-grained samples at a relatively low sintering temperature. The physicochemical properties of the samples were studied.

EXPERIMENTAL

Sample Preparation Methods

BZY samples with a nominal composition of $BaZr_{0.8}Y_{0.2}O_{2.9}$ samples were prepared by conventional SSR methods and the sol–gel-based combined ethylenediaminetetraacetic acid (EDTA)-citric (CEC) sol–gel method, respectively.[24,25] For the conventional SSR method, a stoichiometric amount of $BaCO_3$ (Alfa Aesar, 99.8%), ZrO_2 (Alfa Aesar, 99.7%) and Y_2O_3 (Alfa Aesar, 99.9%) were mixed together by ball-milling in ethanol for 24 h. After drying, the obtained powders were pressed into pellets, followed by calcining at 1100°C for 10 h in air with a heating rate of 3°C min^{-1}. The pellets were then ground into powders which were subsequently mixed with 5 wt.% polyvinyl alcohol (PVA) binder and uniaxially pressed into pellets under a pressure of 400 MPa. The green pellets were sintered at 1500°C for 10 h in air with a heating rate of 2°C min^{-1}. For the samples prepared by the CEC method, $Ba(NO_3)_2$ (Alfa Aesar, 99.95%), $ZrO(NO_3)_2{\cdot}xH_2O$ (Alfa Aesar, 99.9%), $Y(NO_3)_3{\cdot}6H_2O$ (Alfa Aesar, 99.9%) were titrated and dissolved into solutions. EDTA (Alfa Aesar, 99%) and citric acid (Alfa Aesar, 99%) were used as chelating and complexing agents, respectively. Ammonium hydroxide (Sigma-Aldrich, NH_3 content 28.0–30.0%) was added to promote the dissolution of EDTA in deionized water. The metal precursors were then stoichiometrically added into the chelating and complexing agents with the molar ratio of metal nitrates:citric acid:EDTA = 1:1.5:1.2. The solution was stirred at room temperature for 24 h to achieve full complexation, followed by heat treatment in a kitchen microwave oven to assist in foaming. The dry foam was subsequently fired at 600°C for 4 h in air to remove organic residue, resulting in light-colored powders. The powder was then calcined at 850°C for 10 h in air with a heating rate of 3°C min^{-1}. The obtained powder was pulverized and mixed with 5 wt.% PVA binder and pressed uniaxially into pellets under 600 MPa. The green pellets were finally sintered at 1500°C for 10 h in air with a heating rate of 2°C min^{-1}.

The TRAS method was applied to both samples with BZY powders prepared from the SSR and CEC methods. The samples were sintered at 1500°C by the reactive sintering strategy to retain a porous microstructure. The samples were subsequently ground into powders and 1 wt.% B_2O_3-Li_2O sintering aid was added followed by re-sintering at 1500°C.

Characterization

An x-ray diffractometer (Rigaku, Japan) with graphite-monochromatized Cu Kα radiation (λ 1.5418 Å) was employed to record the X-ray diffraction (XRD) patterns of the samples. A scanning rate of 2° min^{-1} was employed to characterize the phases of the samples while a slower scanning

rate of 0.4° min^{-1} was used to perform refinement of the XRD patterns. The diffraction patterns were analyzed by performing Rietveld refinement using the "General Structure Analysis System" (GSAS) package and the graphical user interface (EXPGUI).[26,27] The microstructures of the sintered pellets were examined by field emission scanning electron microscopy (FESEM, Zeiss Ultra). The relative density was measured by the Archimedes method and the porosity was estimated using SEM data analyzed with ImageJ software. Conductivity measurements were performed on sintered pellets. The electrodes were prepared on the sample surface by polishing and the application of platinum paste, followed by heat treatment at 950°C for 30 min. Platinum wires were attached to the surfaces of the Pt current collector. Electrical conductivity tests were conducted using a Zahner IM6 electrochemical workstation (ZAHNER-Electrik GmbH & Co., Kronach, Germany) in the frequency range from 0.1 Hz to 8 MHz at different testing environments. The conductivity measurement was carried out in dry air (dynamic air flowing through a silica gel and a $CaSO_4$ sand), wet air and wet H_2 (both containing 3 vol.% H_2O, obtained by flowing gases through a water bubbler at room temperature) at a temperature range of 400–700°C. Thermal behaviors of the samples were characterized by a NETZSCH DIL 402C pushrod dilatometer from room temperature to 1500°C with a heating rate of 3°C min^{-1}.

RESULTS AND DISCUSSION

XRD Analysis

Figure 1a shows the XRD patterns of the SSR sample calcined at 1100°C, and CEC sample calcined at 850°C, respectively. Trace amount of $BaCO_3$ and ZrO_2 were detected in addition to the main BZY phase. As the literature has reported,[23] the existence of $BaCO_3$ is necessary for the reactive sintering process. Figure 1b shows the XRD spectra of the samples sintered at 1500°C, as well as those sintered by the TRAS method at 1500°C for 10 h. All samples displayed a pure perovskite structure without the presence of secondary phases. Detailed analysis of BZY mixed with Si powder as an internal reference standard was conducted to determine accurate peak positions for the XRD patterns. Rietveld refinement of the XRD patterns as shown in Fig. 2 confirmed the decrease of the lattice parameter due to the introduction of the B-Li sintering aid and followed by re-sintering. Detailed refinement results are summarized in Table I. The introduction of the B-Li sintering aid does not introduce impurities on the XRD patterns as seen for the SSR_TRAS and the CEC_TRAS samples. However, the introduction of small B and Li ions into BZY does lead to shrinkage of the BZY lattice. The possible evaporation of the B-Li sintering aid during the sintering process will also result in a smaller amount of the B-Li sintering aid in the materials compared with the targeted compositions.

Microstructural Analysis

Figure 3 displays the SEM images of the starting powders for the (a) CEC sample, and (b) SSR sample. The CEC sample shows a porous, foam-like morphology coming from the evaporation and burning of the precursor solution. In comparison, the SSR powder shows a uniform distribution of particles with a particle size of 0.2–0.5 μm. The different morphologies of the starting powders had an impact on the microstructure of the sintered samples. Figure 4 shows the cross-sectional SEM pictures of the precursor pellets and the samples fabricated using the TRAS method sintered at 1500°C for 10 h. It can be seen from Fig. 4a that the precursor SSR sample prepared by an SSR sintering method at 1500°C for 10 h shows a porous microstructure. The porosity was measured from the SEM images to be approximately 23.3% (See Fig. S1) with an average grain size of 0.82 μm and a relative density of 71.3% measured by Archimedes'

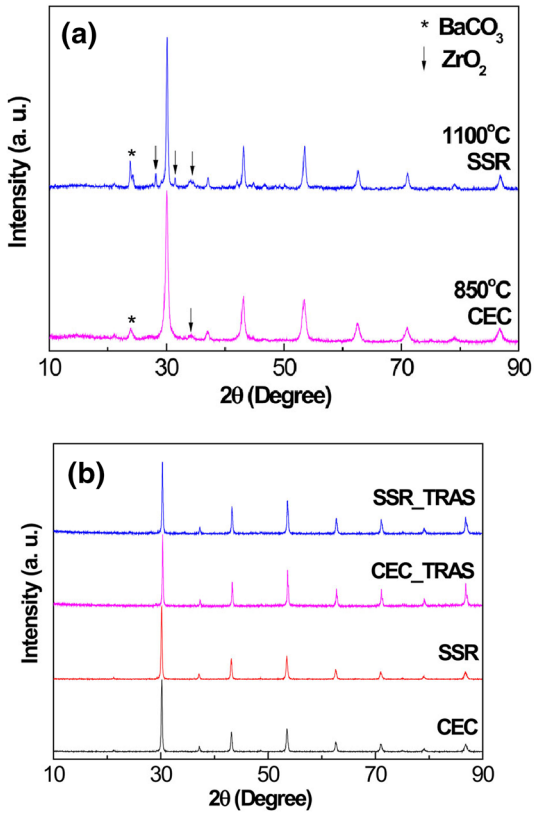

Fig. 1. XRD patterns of BZY samples (a) calcined precursor samples, (b) the samples sintered at 1500°C. CEC_TRAS: sample prepared by the CEC method and re-sintered by the TRAS method with the introduction of the B-Li sintering aid; SSR_TRAS: sample prepared by the SSR method and re-sintered by the TRAS method with the introduction of the B-Li sintering aid.

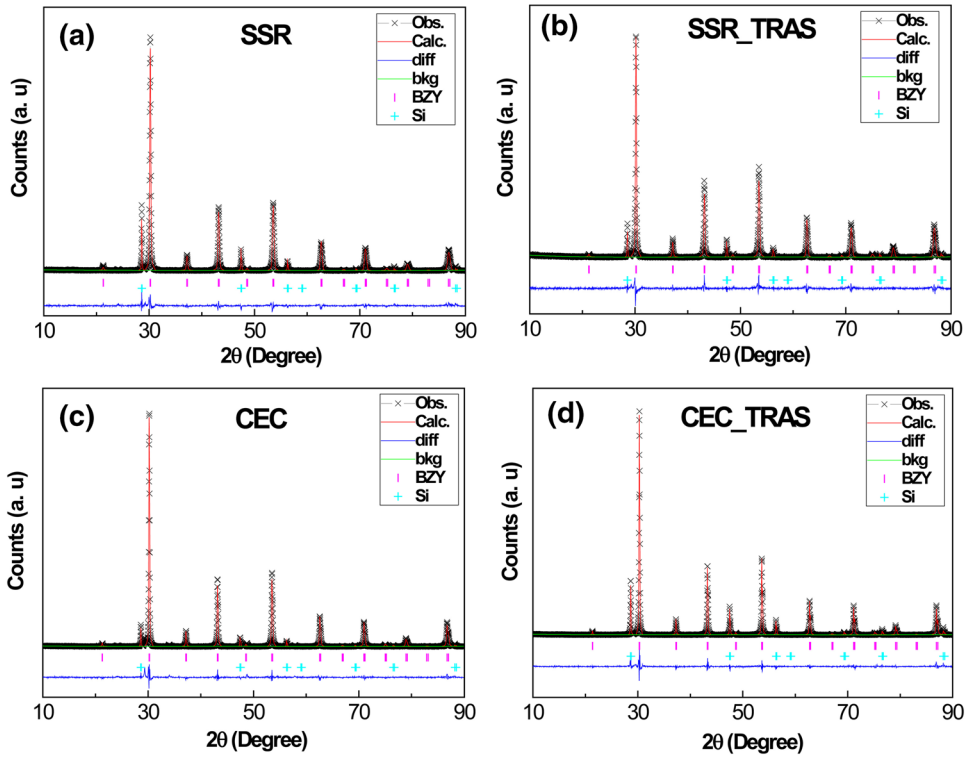

Fig. 2. Rietveld refinement result for the XRD patterns of samples mixed with Si employed as an internal reference standard: (a) SSR sample pellet as prepared, (b) SSR sample prepared by the TRAS method, (c) CEC sample pellets as prepared, (d) CEC sample prepared by the TRAS method (Color figure online).

Table I. Structural parameters for the samples by XRD diffraction fitted by Rietveld refinement

Parameters	CEC	SSR	CEC_TRAS	SSR_TRAS
a (Å)	4.2043(8)	4.20009(9)	4.19851(6)	4.1990(1)
R_{wp}	0.1402	0.1078	0.1170	0.1258
R_p	0.0926	0.0813	0.0906	0.1013
χ^2	3.732	3.153	2.655	2.261

method. Samples sintered by the TRAS method under the same conditions (1500°C for 10 h) exhibited a fully densified microstructure, as shown in Fig. 4b, with an average grain size of 1.03 μm and a relative density of 91.5%. The CEC sample prepared by the sol–gel method displayed a microstructure similar to the sample prepared by the SSR method (porosity of 33.4%, see Fig. S2); however the grain size was smaller, at approximately 0.30 μm (Fig. 4c) and the relative density was found to be 81.5%. As shown in Fig. 4d, the CEC sample prepared by the TRAS method also exhibited a dense microstructure, with an average grain size of 0.45 μm and a relative density of 88.2%. It is clear that the addition of the B-Li sintering aid effectively improved the densification and microstructure as well as the final size of the crystalline grains, even though the maximum sintering temperature remained the same during the re-sintering process.

Sintering Behavior

Figure 5 shows the sintering behavior of the samples with different preconditions for the dilatometry measurement. It can be seen that for the precursor BZY sample prepared by the SSR method, the shrinkage was 8.5%, up to 1550°C (Black). After the addition of the 1 wt.% B-Li sintering aid to the sintered precursor sample, a shrinkage rate of 19.3% was achieved (Red). The precursor BZY sample prepared by the CEC method showed a similar trend, with the precursor sample shrinking 13.9% (Green), while the TRAS exhibited shrinkage on the order of 11.4%, a value slightly less than that of the precursor CEC sample (Blue). In order to affect a comparison between these samples, the SSR sintered pellet was ground and pressed into pellet again for dilatometry measurement. A low shrinkage rate of 2.6% was obtained (which

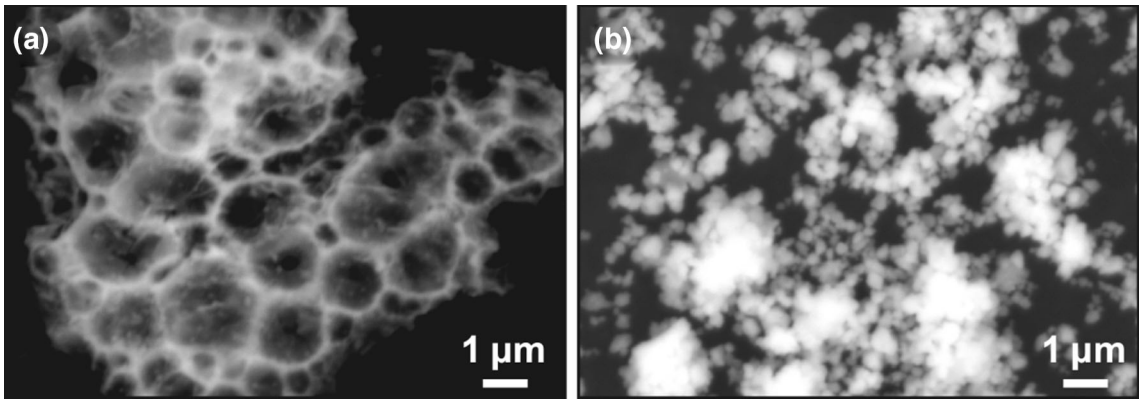

Fig. 3. SEM images of sample powders for (a) CEC sample powder heated at 850°C, (b) SSR sample calcined at 1100°C.

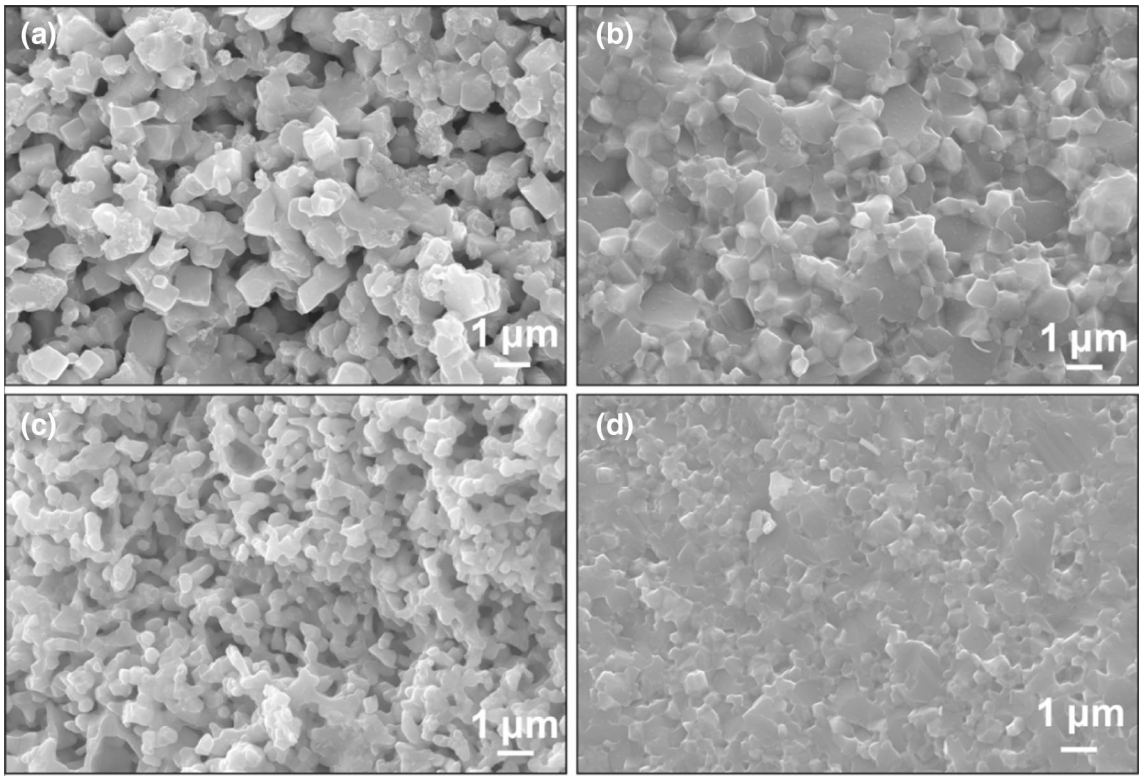

Fig. 4. Cross-sectional SEM pictures of sample pellets sintered at 1500°C for 10 h: (a) SSR sample pellet as prepared, (b) SSR sample prepared by the TRAS method, (c) CEC sample pellets as prepared, (d) CEC sample prepared by the TRAS method.

was caused by the burn-out of the organic binders). This behavior was expected and the results can be considered as re-sintering the sintered sample (Magenta), which has little effect on improving the sintering behavior of the material. Considering the preconditions of the TRAS samples, which were both pre-sintered at 1500°C for 5 h, the shrinkage rates obtained from the TRAS method are remarkable.

An analysis of the shrinkage rate curves of the samples shown in Fig. 5 revealed that the TRAS method facilitated the densification at a temperature of approximately 1000°C and the maximum shrinkage rate was achieved at 1125°C. In samples where the TRAS method was not used, the shrinkage was observed to begin at ~1300°C for the CEC and at ~1500°C for the SSR sample. These results confirm that the TRAS method was successful at achieving densified ceramics at a lower temperature as compared to traditional sintering procedures.

Electrical Properties

The electrical properties of the samples were obtained from the alternating current (AC) impedance spectra. Figure 6 shows the typical Nyquist plots of

the CEC sample tested under dry air at different temperatures. The impedance spectra typically involve three semi-circles corresponding to the bulk, grain boundary and electrode responses from high to low frequencies. The three semicircles can be modeled using a parallel R-CPE (constant phase element) equivalent circuit model. With an increase in the testing temperature, the semi-circle corresponding to the bulk conduction response gradually disappears. The bulk resistance is then derived from the high frequency intercept of the intermediate arc with the real axis (as shown in Fig. 6 inset).

Figure 7 shows the total conductivity of the sintered samples in different atmospheres. It can be seen from Fig. 7a that the SSR sample shows a typical proton-conducting behavior. In the lower-temperature regime (below 600°C), the sample tes-

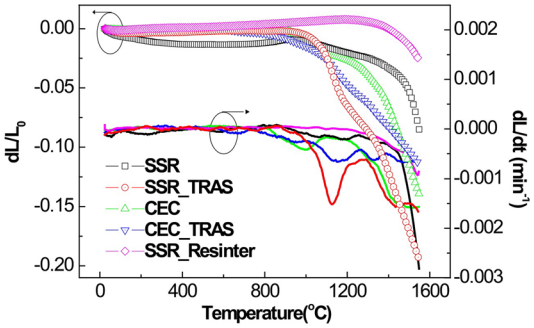

Fig. 5. Sintering behaviors of the samples prepared via different procedures. Black: SSR sample precalcined at 1100°C, Red: SSR_TRAS sample pre-sintered at 1500°C, with 1 wt.% B-Li sintering aid added, Green: CEC sample precalcined at 850°C; Blue: CEC_TRAS sample pre-sintered at 1500°C, with 1 wt.% B-Li sintering aid added; Magenta: SSR sintered pellet, ground, and pressed into pellet again for dilatometry measurement (Color figure online).

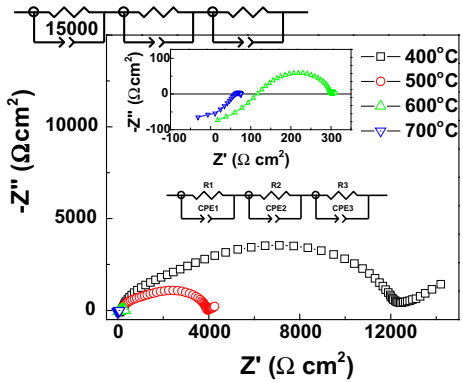

Fig. 6. Typical Nyquist plots of CEC sample tested in dry air (Color figure online).

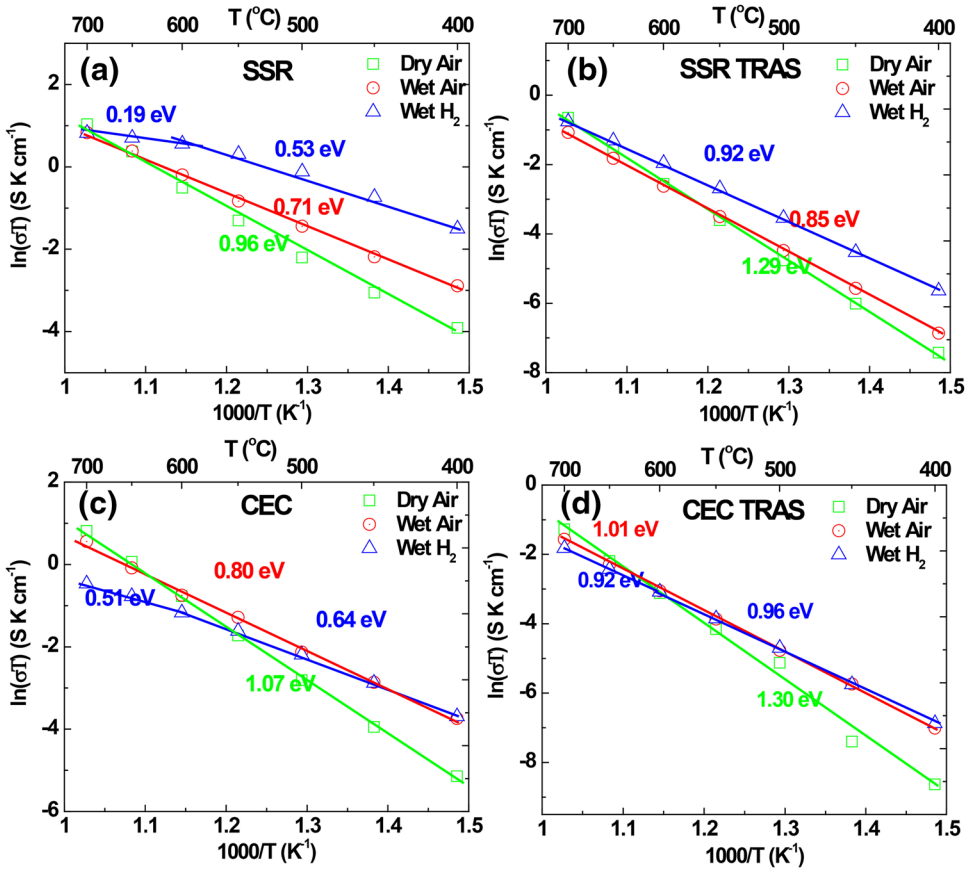

Fig. 7. Total conductivity of the sintered samples in different atmospheres (Color figure online).

Table II. Sinterability, conductivity values (at 500°C) and activation energy values of BZY samples

Sample	Sintering condition	Grain size (μm)	Total (S cm^{-1})	Bulk (S cm^{-1})	Grain boundary (S cm^{-1})	Atmos.	Ea (eV)	Ref.
BZY20-SSR	1500°C, 10 h, oxides	1	1.4×10^{-4}	2.1×10^{-3}	1.5×10^{-4}	Dry air	0.96	This work
BZY20-B-Li	1500°C, 10 h, oxides	1	1.1×10^{-5}	2.4×10^{-3}	1.1×10^{-5}	Dry air	1.29	This work
BZY20-CEC	1500°C, 10 h, nitrates	0.35	7.8×10^{-5}	2.1×10^{-3}	8.1×10^{-5}	Dry air	1.07	This work
BZY20-B-Li	1500°C, 10 h, nitrates	0.35	7.7×10^{-6}	4.1×10^{-3}	7.7×10^{-6}	Dry air	1.3	This work
BZY20-ZnO	1325°C, 10 h,	–	4.8×10^{-4}	7.6×10^{-4}	1.5×10^{-3}	Wet 5% H_2/Ar	0.23	Irvine[15]
BZY20-Li	1600°C, 6 h, wet chemistry nitrates	0.43	2.7×10^{-3}	3.5×10^{-3} (350°C)	7.4×10^{-4} (350°C)	Wet 10% H_2/Ar	0.48	Traversa[20]
BZY20	1600°C, 24 h reactive sintering, nitrates	1	2.2×10^{-2}	1.2×10^{-2} (350°C)	1.0×10^{-2} (350°C)	wet N_2 or Ar	–	Haile[23]
BZY20	1500°C, 20 h, alkoxides	0.2	4×10^{-3}	–	–	Wet Ar	0.54	Cervera[29]

ted in wet H_2 had the highest conductivity and the lowest activation energy, while the sample tested in dry air possessed the highest activation energy. The proton conductivity was enhanced by the introduction of H_2 and water. The proton concentration decreases with an increase in temperature, caused by the dehydration of the materials due to the exothermic nature of the Kröger–Vink reaction

$$H_2O_{(g)} + O_O^{\times} + V_O^{\cdot\cdot} = 2OH_O^{\cdot} \quad (1)$$

where $O_O^{\times}$ refers to neutral oxygen sites, $V_O^{\cdot\cdot}$ to oxygen vacancy, and $OH_O^{\cdot}$ indicates the proton charge carrier formed within the structure by incorporation into the oxygen lattice. This dehydration behavior resulted in decreased activation energy at high temperatures in wet H_2, resulting in a bowed shape for the conductivity curve. A decrease in the activation energy was also observed in the CEC sample, as shown in Fig. 7c. However, the curvature behavior was not found in the TRAS samples. It is believed that the introduction of the B-Li sintering aid leads to the higher activation energy due to the insulating nature of this compound towards the transport of ionic defects associated with proton conduction in oxides. The conductivity values are approximately one order of magnitude lower than the values without the sintering aid. Detailed results are shown in Table II.

The bulk and grain boundary conductivity were separated from impedance measurements and are presented in Fig. 8. For the bulk conduction, the activation energies ranged from 0.48 eV to 0.61 eV, which is characteristic of ionic conduction. For the CEC_TRAS samples, improved bulk conductivity was achieved over the entire temperature range of testing. For the SSR_TRAS sample, improved conductivity was observed at temperatures higher than 500°C due to the higher activation energy of the sample. The improved bulk conductivity was due to the improved densification conditions of the TRAS samples where the densified microstructure with larger grains exhibits a higher proportion of bulk conductivity. Assuming that B and/or Li ions are incorporated into the B site of the perovskite structure (with the Shannon ionic radii of the B-site cations, $r_{Zr} = 0.72$ Å, $r_B = 0.27$ Å, $r_{Li} = 0.76$ Å, respectively[28]), increased vacancy concentrations on both Ba and oxygen sites are expected, which may result in improved ionic conductivity according to the following defect reactions[13]:

$$B_2O_3 \xrightarrow{BaZrO_3} 2B'_{Zr} + 3O_O^{\times} + 2V''_{Ba} + 3V_O^{\cdot\cdot} \quad (2)$$

which indicates the introduction of B_2O_3 results in oxygen barium non-stoichiometry, or

$$2BaO + B_2O_3 \xrightarrow{BaZrO_3} 2B'_{Zr} + 5O_O^{\times} + 2Ba_{Ba}^{\times} + V_O^{\cdot\cdot} \quad (3)$$

which suggests that the doping of B_2O_3 consumes BaO in the compound. A similar situation may happen with the introduction of Li_2O:

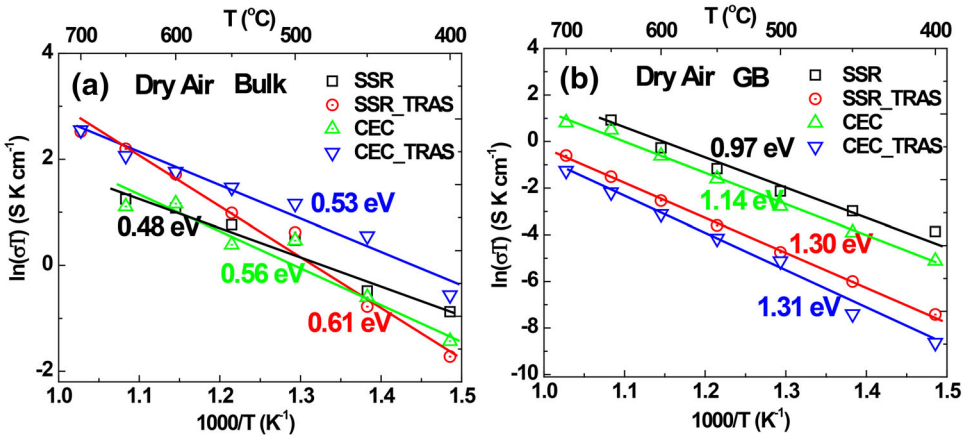

Fig. 8. The bulk and grain boundary (GB) conductivity of the samples tested in dry air (Color figure online).

$$Li_2O \xrightarrow{BaZrO_3} 2Li'''_{Zr} + O_O^{\times} + 2V''_{Ba} + 5V_O^{\cdot\cdot} \quad (4)$$

or

$$2BaO + B_2O_3 \xrightarrow{BaZrO_3} 2B'_{Zr} + 5O_O^{\times} + 2Ba_{Ba}^{\times} + V_O^{\cdot\cdot} \quad (5)$$

Consistent with the XRD results, the introduction of the B-Li sintering aid led to a shrinkage of the lattice. Regarding the likely defect mechanisms, Eqs. 2 and 3 would be the simplest situation resulting if only Boron ions doped into the B-sites. The situation described in Eqs. 4 and 5 would not happen alone since the ionic radius of Li^+ is larger than Zr^{4+} with a coordination number of 6 based on Shannon radii.[28] However, Eqs. 4 and 5 may occur together with Eqs. 2 and 3, with the combined effect of a decreased lattice parameter. There is also the possibility that the B and/or Li ions may be doped into the interstitials of the BZY structure.

Differences also exist in the grain boundary conductivity as a function of processing conditions. The grain boundary conductivity of the SSR and CEC samples are generally one order of magnitude higher than their TRAS counterparts. The activation energy values are also lower, with ~1 and 1.3 eV for SSR and CEC samples, respectively. This result is consistent with observations that the sintering aid improved the grain boundary migration during the sintering process, while at that same time contributed to the reduction in grain boundary conductivity due to the insulating nature of the sintering aid. It is also of note that the SSR samples displayed higher grain boundary conductivity than the CEC samples, for both the conventional and TRAS methods, indicating that the larger grains are beneficial for the grain boundary conduction.

For our TRAS sample, the bulk conductivity is among the highest level reported in this material system (10^{-3} S cm^{-1} at 500°C), which is due to the large-grained, dense microstructures of the sample. However, the grain boundary conductivity is approximately one order of magnitude lower than the bulk conductivity (and one to three orders of magnitude lower than the literature results), which reduces the total conductivity. Consequently, the B-Li sintering aid is believed to be segregated at the grain boundaries, so that the ionic conduction was blocked by a grain boundary impurity phase. Although the grain boundary impurity phase improved the sinterability of the ceramics, and thus enhanced the bulk conduction, the sintering aid also exhibited a blocking effect that lowered the grain boundary conductivity. The combined effect resulted in lowered total conductivity.

CONCLUSIONS

Densified BZY samples were successfully prepared by a TRAS method with a B-Li sintering aid. The first reactive sintering step at 1500°C introduced $BaCO_3$ and the sample reached a density of ~70%. The introduction of B_2O_3-Li_2O sintering aid during the second sintering step at 1500°C produced fully densified BZY ceramics. The structure remained in a pure phase with a reduced lattice parameter due to the introduction of the B-Li sintering aid. The bulk conductivity was improved due to the dense microstructure with a large grain size resulting in the highest bulk conductivity levels reported in this material system. The TRAS method is, thus, a promising way to produce dense, large-grained ceramic oxides due to its simplicity and effectiveness. However, investigation of the optimized composition, concentration and mechanism of incorporation of the B-Li sintering aid is needed in order to balance the densification of the sample and the deterioration of the grain boundary conductivity.

ACKNOWLEDGEMENT

We gratefully acknowledge the financial support from the SCUREF/SRNS/DOE under Award #

B139006. Y. Chen thanks the support from Materials, Science and Engineering Division, Office of Basic Energy, Sciences, Office of Science, U.S. Department of Energy. K. Brinkman acknowledges the Energy Frontier Research Center on Science Based Nano-Structure Design and Synthesis of Heterogeneous Functional Materials for Energy Systems (HeteroFoaM Center) funded by the U.S. Department of Energy, Office of Science, Office of Basic Energy Sciences (Award No. DE-SC0001061). K. Brinkman also wishes to acknowledge a 2014 Clemson TIGER Grant on Materials and Processes for Natural Gas Utilization.

ELECTRONIC SUPPLEMENTARY MATERIAL

The online version of this article (doi: 10.1007/s11664-015-4078-9) contains supplementary material, which is available to authorized users.

REFERENCES

1. H. Iwahara, T. Esaka, H. Uchida, and N. Maeda, *Solid State Ion.* 3–4, 359 (1981).
2. K.D. Kreuer, *Annu. Rev. Mater. Res.* 33, 333 (2003).
3. L. Yang, S.Z. Wang, K. Blinn, M.F. Liu, Z. Liu, Z. Cheng, and M.L. Liu, *Science* 326, 126 (2009).
4. E. Fabbri, L. Bi, H. Tanaka, D. Pergolesi, and E. Traversa, *Adv. Funct. Mater.* 21, 158 (2011).
5. S. Wang, L. Zhang, L. Zhang, K. Brinkman, and F. Chen, *Electrochim. Acta* 87, 194 (2013).
6. S. Wang, Y. Chen, S. Fang, L. Zhang, M. Tang, K. An, K. Brinkman, and F. Chen, *Chem. Mater.* 26, 2021 (2014).
7. S. Fang, S. Wang, K. Brinkman, and F. Chen, *J. Mater. Chem. A* 2, 5825 (2014).
8. J. Tong, D. Clark, L. Bernau, M. Sanders, and R. O'Hayre, *J. Mater. Chem.* 20, 6333 (2010).
9. S. Wang, L. Zhang, Z. Yang, L. Zhang, S. Fang, K. Brinkman, and F. Chen, *J. Power Sources* 215, 221 (2012).
10. S. Wang, F. Zhao, L. Zhang, K. Brinkman, and F. Chen, *J. Alloys Compd.* 506, 263 (2010).
11. C.D. Savaniu, J. Canales-Vazquez, and J.T.S. Irvine, *J. Mater. Chem.* 15, 598 (2005).
12. S. Wang, Y. Liu, J. He, F. Chen, and K. Brinkman, *Int. J. Hydrog. Energy* 40, 5707 (2015).
13. P. Babilo and S.M. Haile, *J. Am. Ceram. Soc.* 88, 2362 (2005).
14. S.W. Tao and J.S. Irvine, *Adv. Mater.* 18, 1581 (2006).
15. S. Tao and J.T.S. Irvine, *J. Solid State Chem.* 180, 3493 (2007).
16. D. Gao and R. Guo, *J. Alloys Compd.* 493, 288 (2010).
17. S. Le, J. Zhang, X. Zhu, J. Zhai, and K. Sun, *J. Power Sources* 232, 219 (2013).
18. X. Chou, J. Zhai, J. Sun, and X. Yao, *Ceram. Int.* 34, 911 (2008).
19. S.W. Wang, J.W. Zhai, X.J. Chou, and X. Yao, *J. Funct. Mater.* 40, 767 (2009).
20. Z. Sun, E. Fabbri, L. Bi, and E. Traversa, *Phys. Chem. Chem. Phys.* 13, 7692 (2011).
21. J. Tong, D. Clark, M. Hoban, and R. O'Hayre, *Solid State Ion.* 181, 496 (2010).
22. S. Ricote, N. Bonanos, A. Manerbino, and W.G. Coors, *Int. J. Hydrog. Energy* 37, 7954 (2012).
23. Y. Yamazaki, R. Hernandez-Sanchez, and S.M. Haile, *Chem. Mater.* 21, 2755 (2009).
24. S. Wang, F. Zhao, L. Zhang, K. Brinkman, and F. Chen, *J. Power Sources* 196, 7917 (2011).
25. L. Zhang, Z. Mao, J. Thomason, S. Wang, and K. Huang, *J. Am. Ceram. Soc.* 95, 1832 (2012).
26. A.C. Laurson and R.B. Von Dreele, *General Structure Analysis System (GSAS)* (Los Alamos: Los Alamos National Laboratory Report LAUR, 2004), pp. 86–748.
27. B. Toby, *J. Appl. Crystallogr.* 34, 210 (2001).
28. Database of Ionic Radii, http://abulafia.mt.ic.ac.uk/shannon/ptable.php. Accessed 23 August 2015.
29. R. Cervera, Y. Oyama, S. Miyoshi, K. Kobayashi, T. Yagi, and S. Yamaguchi, *Solid State Ion.* 179, 236 (2008).